

Influence of surfactants on the electrohydrodynamic stretching of water drops in oil

Åsmund Ervik^{a,*}, Torstein Eidsnes Penne^b, Svein Magne Hellesø^c,
Svend Tollak Munkejord^c, Bernhard Müller^a

^a*Department of Energy and Process Engineering, Norwegian University of Science and Technology (NTNU), 7491 Trondheim, Norway*

^b*Department of Physics, Norwegian University of Science and Technology (NTNU), 7491 Trondheim, Norway*

^c*SINTEF Energy Research, P.O. Box 4761 Sluppen, 7465 Trondheim, Norway*

Abstract

In this paper we present experimental and numerical studies of the electrohydrodynamic stretching of a sub-millimetre-sized salt water drop, immersed in oil with added non-ionic surfactant, and subjected to a suddenly applied electric field of magnitude approaching 1 kV/mm. By varying the drop size, electric field strength and surfactant concentration we cover the whole range of electric capillary numbers (Ca_E) from 0 up to the limit of drop disintegration. The results are compared with the analytical result by G.I. Taylor (*Proc. R. Soc. A* **280**, 383 (1964)) which predicts the asymptotic deformation as a function of Ca_E . We find that the addition of surfactant damps the transient oscillations and that the drops may be stretched slightly beyond the stability limit found by Taylor. We proceed to study the damping of the oscillations, and show that increasing the surfactant concentration has a dual effect of first increasing the damping at low concentrations, and then increasing the asymptotic deformation at higher concentrations. We explain this by comparing the Marangoni forces and the interfacial tension as the drops deform. Finally, we have observed in the experiments a significant hysteresis effect when drops in oil with large concentration of surfactant are subjected to repeated deformations with increasing electric field strengths. This effect is not attributable to the flow nor the interfacial surfactant transport.

Keywords: electrohydrodynamics, droplet, surfactants

PACS: 47.11.-j, 47.15.G-, 47.55.D-, 47.55.dk, 47.65.-d

*Corresponding author

Email address: asmunder@pvv.org (Åsmund Ervik)

1. Introduction

Surfactants are ubiquitous in two-phase fluid flows. Take for instance a single drop falling through a viscous fluid, perhaps the simplest and most widely studied two-phase flow configuration. While the classic results by Hadamard (1911) and Rybzyński (1911) give the analytical result for the flow field in this case, experimental investigations mostly fail to agree with this result. The discrepancy is attributed to trace surface-active contaminants, found even in the most purified of liquids. It is natural, then, also to consider the effects of surfactants on the more complicated case of electrohydrodynamic deformation of a conducting drop falling in an insulating oil.

The case of a drop deforming in an electric field is interesting, not only as an intriguing physical phenomenon of which our understanding can be improved, but also for applications e.g. to chemical processing equipment such as electrocoalescers (Atten, 1993; Eow *et al.*, 2001; Lundgaard *et al.*, 2006). A deeper understanding of the physical processes at play in this system could lead to improved coalescer equipment and reduced emissions.

We will consider here experiments and simulations of sub-millimetre-sized drops of brine falling in a highly refined oil with added surfactant, studying the drop deformations and oscillations induced by square voltage pulses of varying amplitude applied to parallel electrodes above and below such a drop.

When performing these studies of drop deformations, it is crucial to have a system which is well characterised in terms of the fluid and the interfacial properties. To overcome the uncertainties associated with unknown trace contaminants acting as surface-active agents, we deliberately add a non-ionic surfactant (Span 80) in known, small quantities. The interfacial tension as a function of surfactant concentration is then measured, together with the bulk properties, to give a well-characterised system.

There is a large amount of research on the deformations of drops in electric fields, using analytical, experimental and numerical techniques; we will not summarise all of it here. The review by Melcher and Taylor (1969) covers the fundamentals in a thorough fashion, while the review by Saville (1997) gives an update with more recent results in the field. However, when surfactants are added to this picture, the literature is not so extensive. Previous authors (Ha and Yang, 1998; Zhang *et al.*, 2015) have investigated the influence of surfactants on the electrohydrodynamic stretching experimentally, but they have been limited to considerations of the static (equilibrium) deformation, as well as drop sizes above 1 mm in diameter, and a limited number of observations. Computational studies in the literature, namely previous work by Teigen *et al.* (2010), and the paper by Nganguia *et al.* (2013) which finds good agreement with Teigen *et al.* (2010), have also been focused on the static deformation. Note that the numerical code used in this paper is the same as in Teigen *et al.* (2010).

Taking a step further, we consider here also the dynamical behaviour of the stretching drops, in particular the effects of the surfactant concentration on the damping of the drop oscillations. We work with drops smaller than 1 mm in

diameter. We report results for many drop deformations, almost 300 for the experiments and 44 representative cases for the simulations.

This work is an extension of our initial investigation (Ervik *et al.*, 2014), where five cases of the electrohydrodynamic deformation of drops in insulating oil were studied. In the present work we have extended this analysis to a parameter study of the factors influencing the deformation and the deviations from the classical result by Taylor (1964), which does not take surfactants into account. The analytical result by Taylor has been found to agree very well with subsequent results, see e.g. Brazier-Smith (1971), and for this reason we use it as a supporting line in the plots and analysis throughout the paper. Following Taylor, we use the dimensionless electric field strength $\zeta = \sqrt{Ca_E}$ in the following.

The results presented here show that the deviation from Taylor’s expression is negligible below dimensionless electric field strengths of $\zeta \approx 0.4$, while above this threshold they become significant. We demonstrate that drops in the presence of surfactants may be deformed beyond the stability limit given by the Taylor theory. Finally we study the effect of the surfactant concentration, and the effects of Marangoni stresses on the damping of drop oscillations. Our results indicate that small concentrations of surfactant give a significant increase in the damping whilst having but a small effect on the equilibrium (static) shape. Also, for the highest surfactant concentration used here, we observe in the experiments a significant hysteresis effect of repeated stretchings. This effect is not seen in the simulations, so it cannot be explained by the hydrodynamics and the surfactant transport processes which are modelled by our approach.

2. Theory

The flow of single-phase oil or water can be described by the incompressible Navier-Stokes equations

$$\nabla \cdot \mathbf{u} = 0, \tag{1}$$

$$\frac{\partial \mathbf{u}}{\partial t} + (\mathbf{u} \cdot \nabla) \mathbf{u} = -\frac{\nabla p}{\rho} + \frac{\eta}{\rho} \nabla^2 \mathbf{u} + \mathbf{f}, \tag{2}$$

where \mathbf{u} is the velocity field, p is the pressure, ρ is the density, η is the dynamic viscosity, and \mathbf{f} is the acceleration caused by some body force, e.g. the gravitational acceleration. This description can be extended to a two-phase flow by incorporating three things, namely that there is an interface separating the two fluids, that the fluids may have different viscosities η_1, η_2 and densities ρ_1, ρ_2 , and finally the effects of interfacial tension and interfacial tension gradients. We mark the drop properties with subscript $_1$ and the bulk properties with $_2$, and denote the interfacial tension by γ . The viscosity difference and the interfacial tension γ contribute to jumps across the interface in various properties such as the pressure; this is detailed in equations (16) to (18) below. Mathematically, this can be incorporated into the Navier-Stokes equations as a singular contribution to \mathbf{f} in equation (2).

This system admits two dimensionless groups, which we may take to be the Reynolds number Re and the Ohnesorge number Oh . The Reynolds number is of interest for a falling drop, where it is defined as $Re_D = \rho_2 u_T D / \eta_2$, u_T being the terminal velocity and D being the drop diameter. For the drops considered here, the Reynolds number is small ($Re_D < 1$), meaning that the inertial term in equation (2) is unimportant for the flow at terminal velocity.

For an oscillating drop, the Ohnesorge number is an important quantity; some authors use the inverse of the Ohnesorge number as the ‘‘oscillation Reynolds number’’ Re_{osc} . We use the definition $Oh = \eta_2 / \sqrt{\rho_2 \gamma D}$, since the ambient fluid is much more viscous for the cases considered here. For the oscillations, the Ohnesorge number is also small ($Oh < 0.2$), but here the inertial term is important since small Oh corresponds to large Re_{osc} .

When considering a single small (i.e. spherical) drop falling in a clean fluid at low Reynolds number, the terminal velocity as well as the flow in the entire domain is given analytically by the results that Hadamard (1911) and Rybzynski (1911) obtained independently,

$$v_{T,HR} = \frac{(\rho_1 - \rho_2) \mathbf{g} D^2 (\eta_1 + \eta_2)}{6\eta_2 (3\eta_1 + 2\eta_2)}. \quad (3)$$

Experimental results for the terminal velocity, however, tend to not agree with this result (see e.g. Bond and Newton, 1928, Fig. 1), but a closer agreement is found with the formula derived by Stokes (1851) for a hard sphere falling in an unbounded domain,

$$v_{T,S} = \frac{(\rho_1 - \rho_2) \mathbf{g} D^2}{18\eta_2}. \quad (4)$$

Indeed Hadamard himself was aware of this discrepancy, as he states in his 1911 paper.

We note that for $\eta_1 < \infty$, the graphs of $v_T(D)$ given by equations (3) and (4) only intersect at $D = 0$, and thus the terminal velocity of a falling drop is an observable quantity that can determine if a system is clean or not. An experimental observation closer to equation (4) indicates a contaminated system, which is indeed the observation for most fluid combinations. It is noteworthy that the experiments which have obtained values agreeing with equation (3) are for quite singular fluid combinations, e.g. mercury drops in glycerine (Levich, 1962).

The currently accepted explanation (see Clift *et al.*, 1978, pp. 35-41) of this phenomenon is that trace contaminants in the system act as surfactants which are swept along the interface by the flow, creating an interfacial-tension gradient which results in a Marangoni force, with the end result that the drop interface is immobile. Since the nature of these trace contaminants are not known, we deliberately add to the oil a known amount of a non-ionic surfactant, Span 80, such that we obtain a well-described fluid system.

The interfacial tension, γ , can be related to the bulk concentration of

surfactant, Λ , using the Szyszkowski (1908) equation of state (EoS):

$$\gamma(\Lambda) = \gamma_0 \left[1 - \beta \ln \left(1 + \frac{\Lambda}{a_L} \right) \right], \quad (5)$$

where γ_0 is the interfacial tension without surfactants, $\beta = R_{\text{gas}} T \Gamma_\infty / \gamma_0$ is the interfacial elasticity, and $a_L = k_{\text{des}} / k_{\text{ads}}$ is the ratio between the adsorption and desorption coefficients of the surfactant. In the expression for β , Γ_∞ is the maximum possible interfacial concentration of surfactant, R_{gas} is the universal gas constant, and T is the temperature (in Kelvin). The parameters β, a_L of this EoS may be computed by fitting to experimental data; note that this also determines Γ_∞ when the temperature is known.

The equilibrium interfacial concentration can subsequently be calculated as

$$\Gamma = \Gamma_\infty \frac{\Lambda}{\Lambda + a_L}. \quad (6)$$

The relationship between interfacial concentration and interfacial tension is then given by the Langmuir EoS:

$$\gamma(\Gamma) = \gamma_0 \left[1 + \beta \ln \left(1 - \frac{\Gamma}{\Gamma_\infty} \right) \right]. \quad (7)$$

For a detailed review of these equations and their derivation, see e.g. (Dukhin *et al.*, 1995, pp. 47–50). In the next section we plot this equation, with parameters obtained by fitting equation (5) to the experimental data of interfacial tension as a function of concentration, together with the experimental data; it is seen that the fit is very good.

In the present case we consider the surfactant to be insoluble, and we restrict ourselves both in simulations and experiments to surfactant concentrations which are below the critical micelle concentration (0.02 wt% for our system). An insoluble surfactant is a good approximation when the time scales for adsorption-desorption are long when compared to the deformation time scales (Pawar and Stebe, 1996; Lucassen-Reynders *et al.*, 2001). This is the case here, since the time it takes to reach equilibrium for the measurements of interfacial tension is in the order of minutes, while the time period of the drop deformations discussed is on the order of milliseconds. We denote the non-equilibrium interfacial surfactant concentration by ξ . The initial value of ξ is given by equation (6), and the concentration profile $\xi(\mathbf{x})$ evolves according to an advection-diffusion equation which is restricted to the interface (see e.g. Xu *et al.* (2006)), namely

$$\frac{\partial \xi}{\partial t} + u_i \frac{\partial \xi}{\partial x_i} - n_i n_j \frac{\partial u_j}{\partial x_i} \xi = D_\xi \left(\frac{\partial^2 \xi}{\partial x_i \partial x_i} - \frac{n_i n_j \partial^2 \xi}{\partial x_i \partial x_j} + \kappa n_i \frac{\partial \xi}{\partial x_i} \right), \quad (8)$$

where we employ the Einstein summation convention. u_i and n_i denotes the components of the velocity \mathbf{u} and the normal vector \mathbf{n} , respectively. $\kappa = \nabla \cdot \mathbf{n}$ is the interfacial curvature. D_ξ is the surfactant interfacial diffusion coefficient,

a parameter which is very difficult to measure. Fortunately the solutions of this equation are quite insensitive to the value of this constant as long as it is small. Here we use the value $5 \cdot 10^{-7} \text{ m}^2/\text{s}$, which is of the same magnitude as that reported e.g. by Sakata and Berg (1969) (albeit for different surfactants).

With this approach, the Gibbs elasticity is taken into account, and its magnitude can be computed as $\beta\gamma$ (Lucassen-Reynders *et al.*, 2001). This only takes into account the elasticity caused by the change in interfacial tension given by a change in the drop area. Other physical mechanisms, such as reorientation of surfactant molecules at the interface, can lead to additional effects, and even cause a phase transition in the surfactant layer (Ravera *et al.*, 2005).

A seminal approach to the stretching of drops by electric fields is the study by Taylor (1964) who did a theoretical analysis of the electrohydrodynamic stretching of a clean conducting drop in a perfect dielectric medium. His result predicts the asymptotic drop deformation as a function of the electric field strength, radius, permittivity of the oil and interfacial tension, all combined into a dimensionless electric field strength ζ . This is equivalent to the square root of the electric capillary number, $\zeta = \sqrt{Ca_E}$, where ζ is defined as

$$\zeta = \bar{E} \sqrt{\epsilon\epsilon_0 D / \gamma}, \quad (9)$$

and \bar{E} is the uniform electric field that is present far away from the drop. Note that papers from that era work in electrostatic units, where the numerical value of ϵ_0 is 1, so it is frequently omitted from their formulae. Note also that some authors use the drop radius rather than the diameter here.

We may compare ζ^2 to the capillary number computed from the terminal velocity, $Ca = \eta_2 u_T / \gamma$, giving us an impression of the relative importance of the external flow versus the electric field as far as the drop shape is concerned. Using numbers relevant to the situation at hand, we estimate a typical value of the hydrodynamic capillary number to be $Ca \approx 0.007$, while a typical value for the electric capillary number is $\zeta^2 \approx 0.25$, indicating that the electric field has a much greater influence on the drop shape than the deformation due to the external flow. One may thus neglect the effects of the external flow when considering the drop deformations.

In his analysis of drop deformation, Taylor considered a clean drop at rest in a medium with the permittivity of free space, approximated the drop shape at equilibrium as ellipsoidal, and assumed that the value of the difference between interfacial tension and electrical stress at the interface is equal at the poles and at the equator. He then derived an implicit formula which predicts the drop elongation a/b as a function of ζ . In this context, a and b denote the semi-major and semi-minor axis of the drop, respectively, see also figure 3b in the next section.

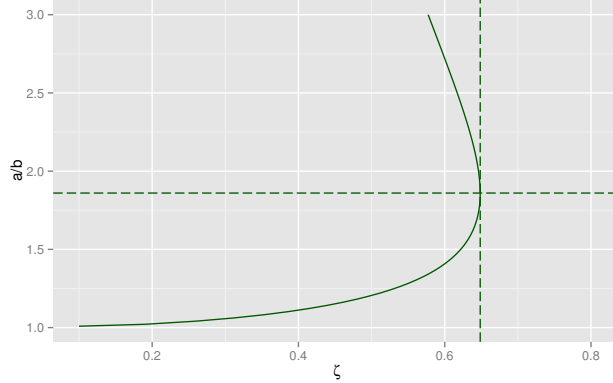


Figure 1: The static deformation predicted by Taylor's theory.

That implicit formula may be given e.g. as the zero level of the function

$$f\left(\zeta, \frac{a}{b}\right) = 2\left(\frac{a}{b}\right)^{-4/3} \sqrt{2 - \left(\frac{a}{b}\right)^{-1} - \left(\frac{a}{b}\right)^{-3}} I - \zeta, \quad (10)$$

$$I = \frac{1}{2} e^{-3} \ln\left(\frac{1+e}{1-e}\right) - e^{-2}, \quad (11)$$

$$e = \sqrt{1 - (a/b)^{-2}}. \quad (12)$$

This predicts a limit to the static deformation at $a/b \approx 1.86$ and $\zeta \approx 0.65$; at higher applied field strengths the drop does not reach an equilibrium state, but is torn apart. Taylor showed that this limit agrees with experiments done with drops in air. The theoretical result by Taylor is shown in figure 1 together with a horizontal line at $a/b = 1.86$ and a vertical line at $\zeta = 0.6485$.

For the numerical model, including the effects of an electric field on the drop requires knowledge of this field inside the simulation domain. Even though we consider a conducting drop in a dielectric medium, we may model the situation as two dielectric media with a very high permittivity ratio (Melcher and Taylor, 1969). We use here a numerical value of 1000 for the relative permittivity of the conducting liquid; this value is not important as long as it is much larger than that of the dielectric liquid. The model validity is confirmed by the fact that the calculated field lines inside the drop are indeed straight, parallel lines in the direction normal to the electrodes, as seen in figure 4b.

To obtain the electric field, we may then proceed by solving a Laplace equation for the electric potential Ψ , with the applied voltage as boundary conditions at the top and bottom of the domain, and $\nabla\Psi \cdot \mathbf{n} = 0$ at the vertical boundaries of the domain. To wit:

$$\nabla \cdot (\epsilon\epsilon_0 \nabla\Psi) = 0, \quad (13)$$

where ϵ is the relative permittivity and ϵ_0 is the permittivity in vacuum. Note that we keep ϵ inside the divergence operator here, even though it is piecewise constant, since this is how the discontinuity is handled by the numerical method.

The Maxwell stress tensor, \mathbf{M} , can then be calculated from the electric field $\mathbf{E} = -\nabla\Psi$. Neglecting the magnetic field, which is not of interest here, we have

$$\mathbf{M} = \epsilon\epsilon_0\left(\mathbf{E}\mathbf{E} - \frac{1}{2}(\mathbf{E} \cdot \mathbf{E})\mathbf{I}\right). \quad (14)$$

This stress gives a spatially varying contribution to e.g. the jump in the pressure across the interface, which will distort a drop from its spherical shape.

All in all, the formulation presented here takes into account the effects of interfacial tension γ , the applied electric field, and the Marangoni effect that arises from an interfacial-tension gradient. The jumps across the drop interface in various properties are then given as (Bjørklund, 2008; Teigen *et al.*, 2010)

$$[[\mathbf{u}]] = 0, \quad (15)$$

$$[[p]] = 2[[\eta]]\mathbf{n} \cdot \nabla\mathbf{u} \cdot \mathbf{n} + \mathbf{n} \cdot [[\mathbf{M}]] \cdot \mathbf{n} - \gamma\kappa, \quad (16)$$

$$[[\Psi]] = 0, \quad (17)$$

$$\begin{aligned} [[\eta\nabla\mathbf{u}]] &= [[\eta]]\left((\mathbf{n} \cdot \nabla\mathbf{u} \cdot \mathbf{n})\mathbf{n}\mathbf{n} + (\mathbf{n} \cdot \nabla\mathbf{u} \cdot \mathbf{t})\mathbf{n}\mathbf{t} \right. \\ &\quad \left. - (\mathbf{n} \cdot \nabla\mathbf{u} \cdot \mathbf{t})\mathbf{t}\mathbf{n} + (\mathbf{t} \cdot \nabla\mathbf{u} \cdot \mathbf{t})\mathbf{t}\mathbf{t}\right) \\ &\quad - (\mathbf{t} \cdot \nabla_\iota\gamma)\mathbf{t}\mathbf{n}, \end{aligned} \quad (18)$$

In these expressions, \mathbf{n} and \mathbf{t} are the normal and tangent unit vectors to the interface. Expressions such as $\nabla\mathbf{u}$ and $\mathbf{n}\mathbf{n}$ denote rank-two tensors formed by the dyadic product, so e.g. $\nabla\mathbf{u} \cdot \mathbf{n}$ denotes such a tensor acting on a vector. We use the convention that a normal vector on a drop points towards the external fluid, and that the jump $[[-]]$ is the difference between the external and the internal properties, e.g. $[[\eta]] = \eta_2 - \eta_1$. The interface is denoted by ι here, so ∇_ι is the gradient along the interface. For the sake of completeness, we mention that an additional term $-(\mathbf{t} \cdot [[\mathbf{M}]] \cdot \mathbf{n})$ contributes to equation (18) when the fluids are not perfect dielectrics, but rather leaky dielectrics. This is considered e.g. by Teigen and Munkejord (2010); Sunder and Tomar (2016), and gives an electric contribution to the tangential force at the interface.

3. Methods

3.1. Experimental methods

Experiments were performed with brine drops (3.36 wt% NaCl added to Milli-Q purified water) immersed in Marcol 52 oil (ExxonMobil), which is a purified and hydrogenated hydrocarbon oil with very low content of surface-active components. Span 80 non-ionic surfactant (Sigma-Aldrich) was added. The densities were measured with an Anton Paar DMA 5000 density meter. The viscosity of the oil was measured with an Anton Paar MCR 102 rheometer.

wt% Span 80	Interfacial tension [mN/m]
0.030	10.0
0.020	10.1
0.015	13.9
0.010	18.8
0.001	29.4

Table 1: Interfacial tension between water and oil for different surfactant concentrations

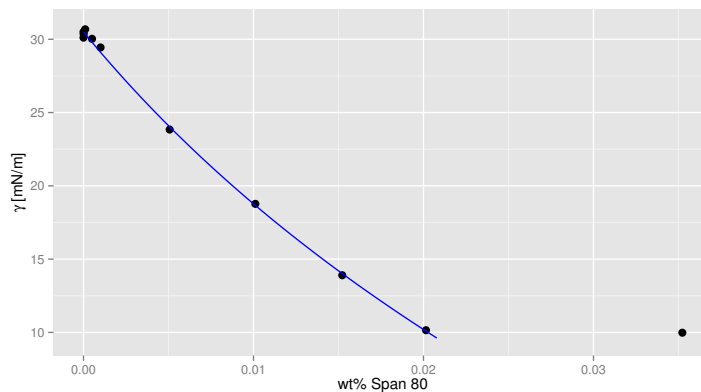


Figure 2: Experimental measurements of interfacial tension (points) and the Langmuir EoS (7) fitted to these (line). Note that the interfacial tension is constant above 0.02 wt%, indicating that this is the CMC.

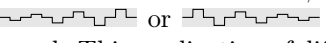
Tabulated values from White (2009) were used for brine viscosity. Experiments were done with temperature control at 21.5°C, where viscosity and density of water were 1.03 mPa·s and 1023.6 kg/m³, respectively, and those of the oil were 12.4 mPa·s and 832.3 kg/m³, respectively. The relative permittivity of Marcol 52 was taken to be 2.13, as per the data sheet supplied by the manufacturer.

Interfacial tension was measured with a SIGMA 703D tensiometer with a DuNuoy ring, for different Span 80-concentrations, with selected values shown in table 1. All data points are given in the supplementary information. Here wt% means weight percent. From these measurements, the critical micelle concentration was determined to be 0.020 wt%, and we limit ourselves to concentrations below this value.

β and a_L in equation (5) were determined by fitting this equation to the experimental measurements using non-linear least-squares. See the plot of the data points and the fitted equation in figure 2; note in particular that the interfacial tension is constant above 0.02 wt%, confirming that this is the critical micelle concentration (CMC). It is somewhat difficult to tell whether the point at 0.02 wt% is a little above or a little below the CMC; thus we have tested the sensitivity of the curve fit to this point by also computing a fit with this point omitted. At the highest concentration studied here, 0.016 wt%, this change

in the curve fit produced a change in the interfacial tension predicted by the EoS of 0.1 mN/m, i.e. less than 1% and within the experimental uncertainty. Accordingly, the small uncertainty about the exact value of the CMC has no influence on the results presented in this paper.

In addition to fitting the EoS, the interfacial area available to each surfactant molecule at the critical micelle concentration, A_{CMC} , was estimated from the slope of the Gibbs isotherm as it approaches the CMC (Tsuji, 1998). For further details, see the supplementary information which contains the script used for fitting and the experimental data. When comparing with the results by Peltonen and Yliruusi (2000), we find good agreement for the values of A_{CMC} and the critical micelle concentration (CMC) obtained here, 30.5 Å² and 0.020 wt%, respectively.

The deformation of the water drops was observed as they fell in the 15 mm gap between an upper and a lower horizontal metal electrode. Drops were produced from a screw-in syringe connected to a glass capillary tube made hydrophobic by a silane coating; this tube protruded through a small hole in the upper electrode. A series of square voltages with different amplitudes was applied to the lower electrode, creating an electric field \mathbf{E} that distorted the drop. The voltage pulse shape was generated in MATLAB and sent over a serial connection to a Stanford Research DS340 signal generator connected to a TREK 2020B high voltage amplifier. The voltage pulse shapes were either rising or falling, and included both positive and negative pulses; i.e. the pulses were bipolar. The length of each pulse was 25 ms, with a 25 ms pause between pulses. The amplitudes were defined as fractions of a maximum amplitude V_0 , e.g. $V_0 = 10$ kV and fractions 2/4, 3/4 and 4/4 times V_0 , giving pulses that look like . Typically 6 different amplitudes (fractions) were used. This application of different voltages resulting in different stretchings of the same drop is the only practical way of studying the effect of varying the electric field strength at constant drop radius. It also allows us to study possible hysteresis effects of the stretching on the surfactant on the interface. Such effects have been reported previously, e.g. by Peltonen and Yliruusi (2000) for the Span 80 surfactant used here.

When applying several voltage pulses to the electrodes it is desirable to keep the drop in the camera field-of-view for as long as possible. To achieve this, a moving stage setup was used, comprised of a Newport (M-)IMS-V linear stage to move the test cell containing the fluid system upwards a constant velocity, and a Newport XPS Series Motion Controller to manually match the velocity of the moving stage to the terminal velocity of the drop.

A side view of the experimental setup is shown in figure 3a, and a 3D rendering is shown in figure 3c. To avoid unnecessary clutter, the temperature control bath, optical setup and the linear stage are omitted in both of these figures, and in figure 3c the cuvette containing oil and the syringe mechanism are also omitted. The drop size relative to the setup is exaggerated in both figures.

To record high-speed movies of a falling drop, a Cheetah CL near-infrared camera was used with an Infinity KS2 long-range microscope lens, and a

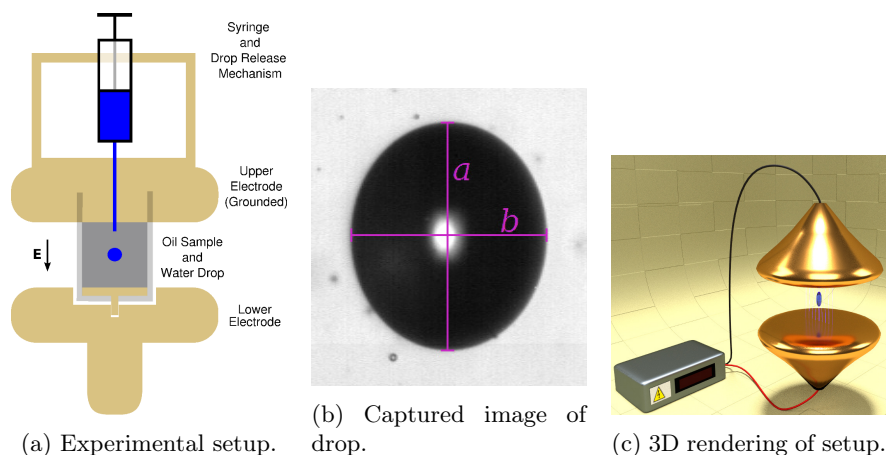


Figure 3: Schematic showing a side view of the experimental setup, an example of a captured drop image shown with the major and minor axes a and b superimposed, and a 3D rendering with a simulated droplet and electric field shown between the electrodes. The drop size is exaggerated in both (a) and (c).

collimated light source was placed on the opposite side of the cuvette. The camera recorded a frame of 640×512 pixels at 1730 frames per second. The high-speed movies were recorded in the Streams 7 software, together with the voltage pulse from the signal generator and the velocity and position of the moving stage. These electrical signals were captured using a National Instruments PCI-6052E DAQ board.

To determine the drop deformations from the high-speed images, the Spotlight image analysis software was used. With this software, the dimensions of the major axis a and minor axis b of a deformed drop can be determined, as seen in figure 3b, where the axes are superimposed on an image of an elongated drop. This then gives the ratio a/b as a measure of the deformation; note that this measure does not make any assumptions about the drop shape. See also the supplemental material in movie 1 which shows a video of a drop deformation cycle together with an animated plot of a/b as a function of time.

The various uncertainties that affected the measurement of a/b were analysed in a fashion similar to that used by Zhao (2009) and Gaussian error propagation was then used to compute the uncertainty in a/b (Moffat, 1988). This uncertainty was found to be independent of a/b , but dependent on the initial drop radius, which is sensible. The relative error in a/b was largest for the smallest drops under consideration, at 3.4%, and smallest for the largest drops considered, at 2.0%.

The experimental procedure for studying the drop deformation in an electric field was comprised of the following steps:

1. Move the test cell using the linear stage such that the tip of the needle used for generating droplets is in the top of the camera's field-of-view. Use the screw-in plunger to create a droplet of the desired size.

2. Wait for 1 minute to allow the equilibration of surfactants at the drop interface. Arm the camera such that it starts recording 10 ms before the first voltage pulse is applied.
3. Use an electromagnet to jerk the glass needle upwards, releasing the drop.
4. As the drop falls through the view of the camera, adjust the upwards velocity of the moving stage to match the terminal velocity of the drop, keeping the drop in the centre of the image. The drop falls for approx. 0.5 seconds before the voltage pulse train is applied, allowing ample time for any initial oscillations to be damped away.
5. Trigger the voltage pulse train. The camera is also controlled by this trigger and records a movie of the drop being deformed.
6. Post-process the recorded movie to extract a , b as functions of time.

A remark is in order with regards to the waiting time for equilibration of surfactants at the drop. As stated, a waiting time of one minute is used in these studies. If we are to compare this with some intrinsic time scale, we may consider $\tau_D = \Gamma^2/(\Lambda^2 D_B)$ (Lin *et al.*, 1990), with Γ taken at some surfactant concentration Λ , say the highest used in these experiments (0.016 wt%). The value of D_B , the bulk diffusion coefficient of Span 80 in Marcol 52 oil, is not known. Since the Span 80 molecule is not much larger than the alkanes in the oil, we may use as a rough estimate the self-diffusion coefficient of the tail of the Span 80 molecule, namely oleic acid, which gives $D_B \approx 10^{-10}$ m²/s (Iwahashi *et al.*, 2007); of the same order of magnitude as e.g. the diffusion coefficient of C₁₂E₆ surfactant in water (Lin *et al.*, 2003). This gives a time scale of $\tau_D \approx 3 \cdot 10^5$ s, i.e. 3.5 days. It would be impractical to wait for such a long time between each drop was produced.

Fortunately, the transport of surfactants to the interface is greatly accelerated once the drop starts falling, since the velocity boundary layer decreases the length of the diffusion boundary layer. Note that the length of the diffusion boundary layer as estimated above is $l = \Gamma/\Lambda = 20\mu\text{m}$, which is comparable to the drop radius of 250–500 μm . To quantify the increase in surfactant transport to the interface, we may consider the Schmidt number, i.e. the ratio between the viscous and the molecular diffusion rates, which in this system is $Sc = 2 \cdot 10^5$. This indicates that the combination of the one minute waiting time and the subsequent falling time of 0.5 s between drop release and the start of the first deformation should be sufficient to ensure the interfacial surfactant concentration is equilibrated before the deformations commence.

3.2. Simulation and numerical methods

An in-house code was used to solve the Navier-Stokes equations (1) and (2) numerically. The simulations reported here are done in axisymmetry. See Teigen and Munkejord (2009); Teigen *et al.* (2010); Teigen and Munkejord (2010) for validation of the methods and implementation used here.

The equations are discretised on a structured, uniform, staggered grid using the finite-difference method. For the convective terms, the fifth-order WENO scheme (Jiang and Peng, 2000) is employed. For the other terms a standard

second-order central-difference scheme is used. The pressure and velocity fields are coupled using the classical projection method due to Chorin (1968), which gives a Poisson equation for the pressure. This Poisson equation is solved here using the BoomerAMG (Algebraic MultiGrid) preconditioner (Henson and Yang, 2000) and the BiCGStab (Bi-Conjugate Gradient Stabilised) iterative solver (van der Vorst, 1992); we use the Hypre (Falgout *et al.*, 2006) and PETSc (Balay *et al.*, 1997) libraries for these methods.

The equations are then integrated in time using an explicit Runge-Kutta method which has the strong stability preserving (SSP) property, namely SSPRK(2,2) in the terminology of Gottlieb *et al.* (2009). Although this method is second order in time, the overall scheme is only first order in time due to the irreducible splitting error from the Chorin projection method. To sum up, the present method is first-order in time and second-order in space.

To capture the position of the interface between the two fluids, the level-set method (Osher and Fedkiw, 2001) is used with the high-order constrained reinitialisation method (Hartmann *et al.*, 2010) and the velocity extrapolation procedure (Adalsteinsson and Sethian, 1999). With the interface position known, the ghost-fluid method (Fedkiw *et al.*, 1999) is used to enforce the jumps specified in equations (16) to (18) across the interface in sharp fashion.

This formulation takes into account the effects of interfacial tension γ , the applied electric field, and the Marangoni effect that arises from an interfacial tension gradient. The surfactant concentration along the interface, ξ , is determined by solving the advection-diffusion equation (8). The interfacial tension γ is then determined by the surfactant concentration according to equation (7), using equation (6) with ξ in place of Λ .

4. Results

4.1. Parameter studies on drop deformation

As stated previously, five distinct cases of drop deformation in the presence of surfactants were studied in our previous paper (Ervik *et al.*, 2014), along with studies on the terminal velocity. Detailed comparisons between the experimental results and the simulation results are given there. In light of the close agreement found, an experimental and a computational parameter study were set up to better understand the effects of surfactants. The aim of the present study is to give a sufficient coverage of the parameter space, and to leverage the combination of simulations and experiments to give a deeper insight. In particular we study the initial drop oscillations when the pulse is applied, and the effect the Marangoni force has on the damping of these oscillations, which has not been studied before. The dataset generated by this study is available in the supplementary information.

For the simulations, a combination of three drop radii, four electric field strengths and four surfactant concentrations was chosen, representative of the parameter ranges used in the experiments. The dimensionless field strength ζ was then computed for each combination, and additional combinations were

	Diameter (μm)	Electric field (V/mm)	Span 80 concentr. (wt%)	ζ (-)
Sim.	(500, 700, 900)	(300, 500, 700, 900)	(0.0, 0.001, 0.005, 0.016)	[0.15 – 0.80]
Exp.	[578 – 902]	[207 – 747]	(0.001, 0.005, 0.016)	[0.15 – 0.65]

Table 2: Ranges for parameters used.

added to ensure a good coverage of the ζ values. The values are summarised in table 2.

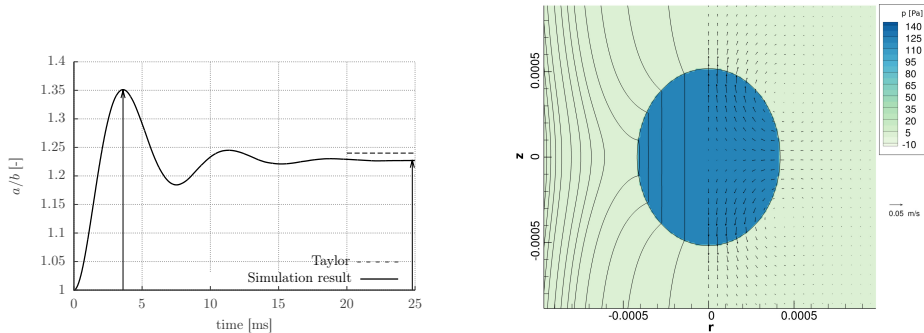
From the experimental point of view, the surfactant concentration is also well-defined at three values (the clean system cannot be reached). The drop radius, on the other hand, is a quantity most difficult to control from one drop to the next, so there is no systematic variation in it. Finally the applied electric field strength is defined from a base value and several fractions of this value, e.g. (2/6, 3/6, 4/6, 5/6, 6/6). This is thus more controlled than the radii. But the base value was varied for different interfacial-tension values, due to a desire to avoid stretching drops beyond their stability limit, as drop destruction necessitates stopping the experimental campaign and cleaning the test cell. The values used in experiments are also summarised in table 2.

It should be noted that the simulations are all done independently, while the experiments are done with several applications of fields of different strength on the same drop. Thus the simulations neglect any hysteresis effects that arise from the hydrodynamics, e.g. if the flow caused by the previous deformation is still significant when the next one commences. Also, since the scaling analysis of the capillary numbers presented in section 2 indicates that gravity (i.e. the external flow due to falling) is unimportant for the deformations, the simulations are performed with zero gravity. Both of these assumptions are confirmed by simulating a falling drop subjected to a rising voltage pulse, showing that neither the simplification of zero-gravity nor that of independent deformations has a significant effect on the simulation results.

In the subsequent sections we show plots of the deformation a/b , as discussed in section 2. During the deformation of a drop, a/b starts as 1, then increases to a peak value, and finally settles at some static value after some oscillations. In figure 4 we plot the time evolution of a/b for one of the cases considered here, as an example. We also show a snapshot of the pressure, velocity and electric fields after 2 ms, which is halfway to the peak deformation. Note that the maximum time in this line plot is the same as the duration of a pulse, so this plot indicates the relaxation towards the new equilibrium of a stretched drop. See also the accompanying movie 1, where a plot like figure 4a from one experiment is shown side-by-side with the high-speed footage of a drop.

4.2. Computational parameter study

In this section we report the results of parameter studies of the deformation as a function of the dimensionless electric field strength. In total 44 cases were studied. The simulations were performed in axisymmetry, using a 241×482 grid covering a $3D \times 6D$ domain. This is about six times larger in each direction than



(a) The deformation, a/b , plotted as a function of time. The peak and static values are pointed out by arrows, and the result by Taylor for the static deformation is shown as a dotted line on the right.

(b) Snapshot of the deforming drop after 2 ms, halfway to the peak deformation. On the right side, velocity vectors are shown for every fifth grid point. On the left side, electric field lines are shown, quadratically spaced due to axisymmetry. The colour indicates pressure.

Figure 4: Example case for $\zeta = 0.52$, a 0.9 mm diameter drop is being deformed by a 700 V/mm field without any surfactants present.

what is shown in figure 4b. As discussed previously we perform the simulations with zero gravity. The initial condition is then a circular drop at rest, with an initial surfactant concentration given by the bulk concentration according to equation (6). The electric field is switched on at $t = 0$; the time it takes in experiments for the voltage to reach its constant value is much smaller than the ~ 0.5 ms it takes for the drop to start deforming. See also the supplemental material in movie 2, where we show an animated 3D rendering produced from one of these simulations, namely of the 900 μm diameter drop in 0.005 wt% Span 80 subjected to a 700 V/mm electric field, corresponding to $\zeta = 0.58$.

The results for the static deformation obtained in the simulations are shown in figure 5. Here the static deformation for each case is shown as a point and compared with the line which is the Taylor result. The points are colour coded by the electric field. The shape of the points indicates the surfactant concentration, and the size of the points indicates the drop radius. The points shown in red were unstable, i.e. the drop stretched until breakup.

As is seen from figure 5, there are deviations from the Taylor theory, occurring mostly for large values of the dimensionless field strength. It is also seen that the dimensionless parameter ζ is still a good variable for describing the system in the presence of surfactants. We note that previous simulations by Brazier-Smith (1971) also find some slight disagreement with the results by Taylor. This is discussed further in section 4.4.

To further study the effects of increasing surfactant concentration on the

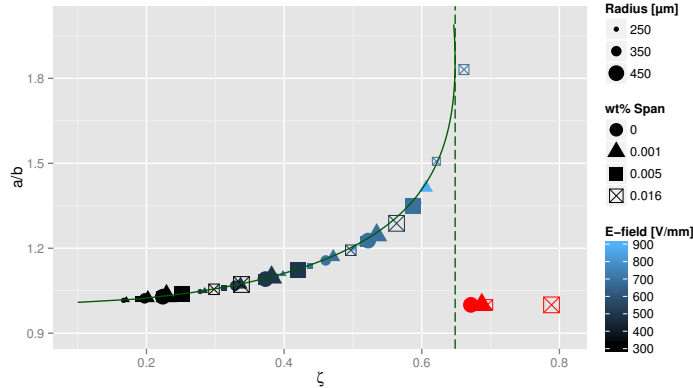


Figure 5: The deformation a/b found in simulations as a function of the dimensionless electric field strength, ζ . Solid line: Taylor theory. Dashed line: static deformation limit. Red points: drop breakup.

oscillation of drops, one may consider the analogy to a damped mass-spring system. In that case, it is more convenient to work with $a - b$ rather than a/b . This is because the former is directly related to the magnitude c_2 of the fundamental mode of the oscillation, given by the coefficient of the second spherical harmonic, *viz.* $a - b = \sqrt{45/16\pi} \times c_2$. Here we assume that essentially only the second spherical harmonic contributes to the oscillation. Note that under the typical assumptions in analytical work on drop oscillations, as used e.g. by Lamb (1932, pp. 473-475), the temporal evolution of c_2 corresponds exactly to the evolution of a damped harmonic oscillator.

Working then with $a - b$ we define the *overshoot* Ω of an oscillation as

$$\Omega = \frac{(a - b)_{\text{peak}} - (a - b)_{\text{static}}}{(a - b)_{\text{static}}}. \quad (19)$$

This is motivated again by analogy with the damped mass-spring system, where the overshoot of the response to a step forcing has a one-to-one correspondence with the damping ratio (Ogata, 2009, p. 172). This measure of the damping is more accurate here than the standard method of fitting an exponential, since the observed oscillations have few discernible peaks. Using the overshoot is less sensitive to uncertainties and can be used even when just one or two peaks are discernible. Using the formula given by Ogata (2009) we compute the damping ratio λ as


$$\lambda = \sqrt{\frac{\ln(\Omega)^2}{\pi^2 + \ln(\Omega)^2}}. \quad (20)$$

Note that it is more traditional in the context of drop oscillations to work with the damping coefficient $b = \lambda \omega_0$, where ω_0 is the natural frequency, as is done by Lamb (1932, p. 474) and by others. This is a bit curious, since their results

predict a damping ratio which is directly proportional to the Ohnesorge number, with a proportionality constant depending on the number of the oscillation mode in question; taking e.g. the result by Lamb for the fundamental oscillation mode of a free droplet we obtain $\lambda = 10/\sqrt{3} \times Oh$. For the damping coefficient b the relationship with Oh also includes ω_0 .

Even though it is known that the oscillations of a viscous drop immersed in a viscous fluid cannot be described by a simple harmonic oscillator (Prosperetti, 1980), we posit here that λ still gives a good measure of how damped the drop oscillations are. Note that it follows from the definition that $\lambda < 1$ corresponds to underdamped oscillations, and that lower values indicate less damped oscillations. In the Supporting Information we plot the oscillations for two cases with the same value of ζ (and thus the same final deformation), but different values of the damping ratio, together with the step responses of harmonic oscillators with the same damping ratios. This plot indicates that λ is a useful measure of the damping.

Having defined this damping ratio λ , we show in figure 6 a plot of λ versus ζ where we connect points with identical drop size and electric field strength. From this plot we may surmise that adding small amounts of surfactant increases the damping significantly, but has a negligible effect on the static deformation (represented here by ζ), so the lines connecting the 0 wt% and the 0.001 wt% results have steep slopes. On the other hand, adding larger amounts of surfactant significantly increases the ζ by reducing γ , so the slopes are flatter. This can be understood when considering that the surfactants play a dual role in the system: adding Marangoni stresses and reducing interfacial tension. From these results we see that when small amounts of surfactant are added, the increase in damping from Marangoni forces is much more significant than the reduction in interfacial tension. When more surfactant is added, the effect of reduced interfacial tension becomes pronounced. We discuss this in more detail in section 4.4, and illustrate the point with detailed plots from the numerical simulations.

Finally, we report the results from a simulation where the drop was falling at terminal velocity and subjected to a rising voltage pulse () matching that used in the experiments. A moving grid procedure was used to keep the falling drop in the centre of the computational domain. The base value of the applied field was 500 kV/m, and the fractions 2/7 to 7/7 of this base value were used.

The surfactant concentration was 0.016 wt% and the drop diameter was 900 μm . Based on the terminal velocity u_T , the capillary number is $Ca_T = \eta_2 u_T / \gamma = 0.004$ and the surface Péclet number is $Pe_T = Du_T / D_\xi = 8.5$. (Recall that D is the drop diameter while D_ξ is the surface diffusion coefficient.) For comparison, the electric capillary number is $Ca_E \in [0.03, 0.3]$ for the increasing field strengths. We may define an electric surface Péclet number, by analogy with the electric capillary number, as $Pe_E = D^2 \bar{E}^2 \epsilon_0 / (\eta_2 D_\xi)$, which gives in this case $Pe_E \in [24, 290]$. All in all, these numbers suggest that the external flow is unimportant, which is also what the simulation results indicate.

The simulation results are shown in figure 7. They are very similar to

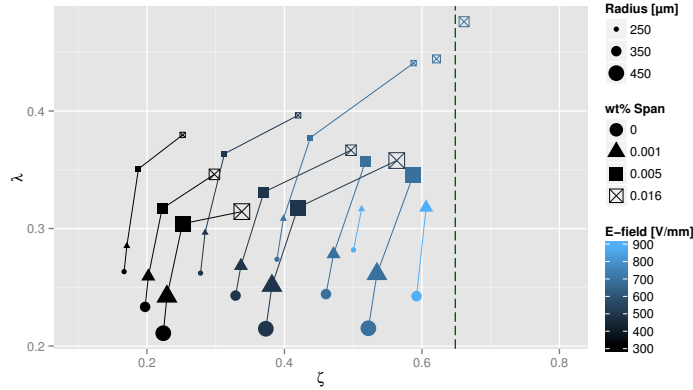

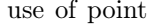


Figure 6: The damping ratio of oscillations, λ , versus ζ . Dashed line: static deformation limit.

those seen in figure 5, which confirms that neither the external flow nor the previous deformations have a significant influence on the static deformation in the simulations. If the hysteresis effect observed in the experiments described in the next section were caused by hydrodynamic effects or by the surfactant transport, e.g. if the flow field was still influenced by the previous deformation at the start of the next deformation, the hysteresis would also be observed in these simulations. Since it is not, these can be ruled out as likely explanations of the hysteresis.

4.3. Experimental parameter study

Several experiments were performed with different drop diameters, field strengths and surfactant concentrations, as described in section 4.1. In total, 295 drop deformations were observed, with 8 to 12 observations of each drop and 4 to 6 different voltages applied with both polarities.

The results for the static deformation obtained in the experiments are shown in figure 8 for rising voltage pulse trains () and figure 9 for falling voltage pulse trains (). The use of point shapes and sizes match those used in figure 5 for the simulations. In these two plots, the shaded region around the Taylor result indicates the magnitude of the uncertainty in the optical observations, as described in section 3.1.

It is seen in these two figures that the experiments are also well-described by the parameter ζ , and that the results lie fairly close to the Taylor theory, especially for low deformations. Below $\zeta \sim 0.4$, the deviations are of the same magnitude as the uncertainty in the optical measurements, while above this, they are significant. In the Supporting Information we plot also the relative deviation Δ from the Taylor theory is plotted.

There is a profound difference seen between rising and falling pulse trains in these plots, in that the deviation is positive for the latter, but both positive

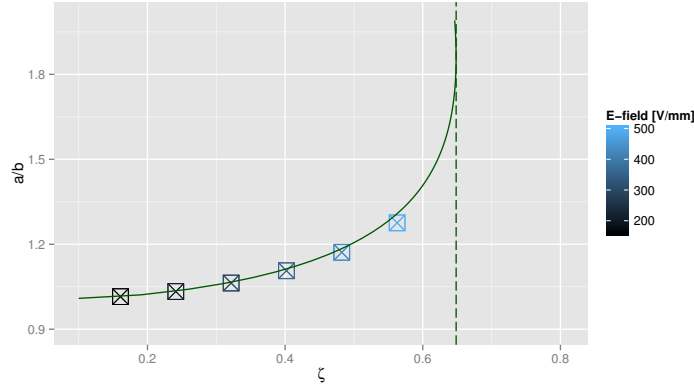


Figure 7: The static deformation a/b versus ζ for a $900 \mu\text{m}$ diameter drop at 0.016 wt% surfactant concentration. This simulation is with a drop falling under gravity and subjected to repeated deformations by a rising voltage pulse.

and negative for the former. Furthermore it is seen that this difference occurs only for the highest concentration of surfactants.

Peltonen and Yliruusi (2000) have reported similar hysteresis effects when repeatedly stretching and compressing an interface between water and hexane with added Span 80, using a Langmuir-Blodgett apparatus. When comparing figure 8 and figure 9 given here, it is noted that for rising voltage pulses, the previous stretchings at small and intermediate field strengths significantly affect the subsequent stretchings, giving a deviation from the Taylor theory that has the opposite sign of that seen in all other cases. Note also that the simulation results (figure 5) show positive deviations for all but one point.

The hypothesis by Peltonen and Yliruusi (2000) is that earlier compressions disperse surfactants into the water phase, but it is not readily apparent that this is the case here; if this were so, the large expansions and compressions of the interface that occur at the beginning of a falling voltage pulse train should significantly affect the subsequent medium and small expansions, but this is not observed.

For the sake of clarity, we remark that the hysteresis seen here is an entirely different phenomenon from the hysteresis studied e.g. by Sherwood (1988). Sherwood considers the hysteresis in the deformation a/b which arises from a finite permittivity ratio, but as is apparent from his figure 2, the phenomenon he discusses requires deformations $a/b \gg 10$, while our deformations are all $a/b < 2$. Thus the hysteresis phenomenon observed herein cannot be attributed to a finite permittivity ratio.

4.4. Comparison of simulations and experiments

Several features of the results of these studies warrant further comment. First of all, we observe stable solutions slightly beyond the limit predicted

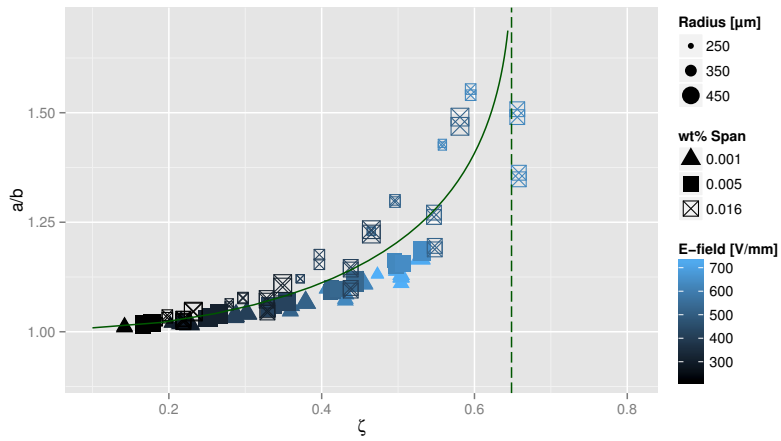


Figure 8: The deformation a/b found in experiments as a function of ζ for **rising** voltage pulse trains. Shaded region: optical measurement uncertainty.

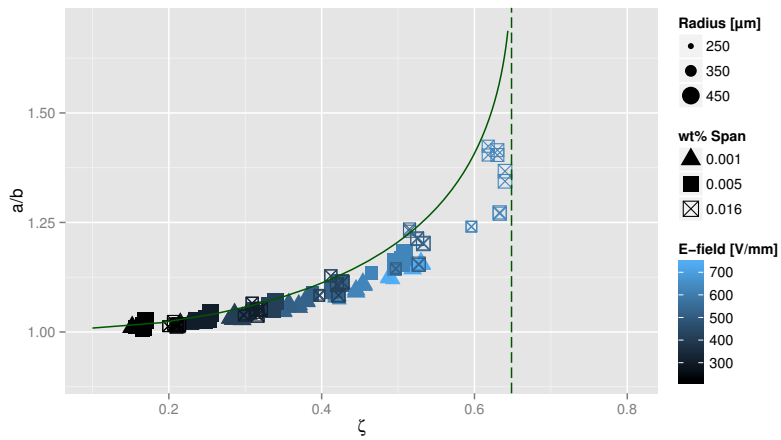


Figure 9: The deformation a/b found in experiments as a function of ζ for **falling** voltage pulse trains. Shaded region: optical measurement uncertainty.

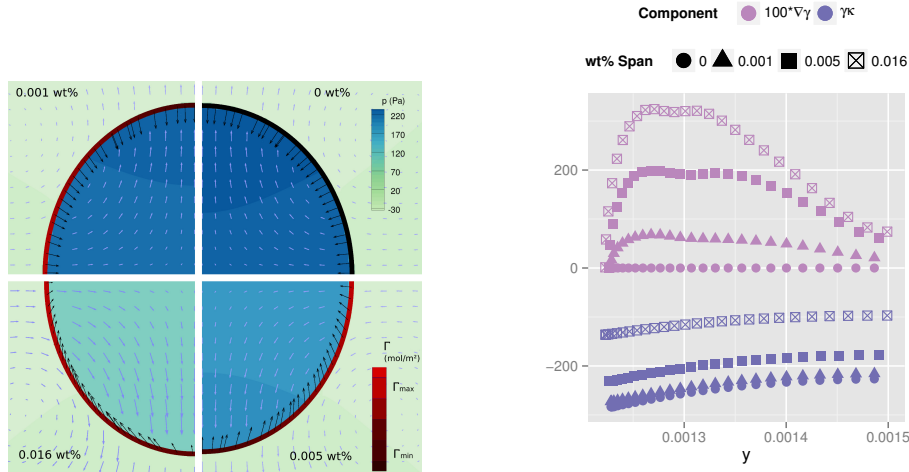
by Taylor. This is attributable to the interfacial elasticity. At the highest surfactant concentration and the largest drop deformations this results in a decrease of about 2% in ζ , which is sufficient to explain the deviation. However, for the lower surfactant concentrations the effect is too small to account for the observed deviation. It is likely that this discrepancy is caused by some of the approximations used by Taylor. Other authors have also pointed out minor disagreements between their results and the Taylor theory. Brazier-Smith (1971), using numerical iterations to obtain pressure balance along the entire interface, found a difference which is very similar to that found here.

As for the general agreement with the Taylor theory, it is apparent from the numerical results that the main effect of surfactants on the static deformation is through the reduction in equilibrium surface tension. When this is taken into account in the calculation of ζ , the results agree nicely with Taylor's prediction, as shown in figure 5.

For the experimental results, however, there is a clear tendency for smaller deformations than those predicted by the Taylor theory. One possibility is that this discrepancy is caused by a form of interfacial elasticity which is not accounted for here, as discussed earlier.

As illustrated in figure 12, the effect of adding surfactant is two-fold. Small additions increase the damping significantly, while the reduction in interfacial tension is small, so the static deformation is not much affected. Conversely, adding larger amounts of surfactants give a significant decrease in interfacial tension causing a larger deformation, while the increase in damping is less significant. In order to explain this effect, we show in figure 10a plots of the pressure field as well as the vector quantity $\gamma\kappa\mathbf{n} - 100 \times \nabla_t \gamma$ at the interface for the four different surfactant concentrations considered here. This is for the 0.5 mm diameter drop subjected to a 700 V/mm electric field. We scale the Marangoni force by 100 to accommodate the visualisation, since the curvature κ is very large for these small drops. The important thing here is not the absolute value of this vector, but rather the comparison between the four cases in the tangential and normal components. All plots are shown at the same time, $t = 1\text{ms}$, which is a little less than halfway to the peak deformation. Around this time, the Marangoni forces are at their largest, since these forces counteract the surfactant maldistribution driving the concentration profile to be uniform at equilibrium. This time is also convenient since the deformation of the drops is very similar at this point in time, while they differ more at later times. Also shown in this plot is the flow field, and the surfactant distribution along the interface in red colour going from the lowest (darkest) to the highest (brightest) concentration along the interface in each case. The interfacial positions are very similar at this early time, which in turn means that both the electric fields and the curvature profiles are also very similar. However, note that the flow is stronger for the drop with the highest surfactant concentration, consistent with the fact that this will be more deformed than the other drops.

In all the three cases where surfactants are present, it is seen that the initial deformation gives an increased surfactant concentration near the equator and a reduced concentration near the poles. The lowest and highest



(a) Comparison of the pressure field (blue/green), the vector $\gamma\kappa\mathbf{n} - 100\nabla_t\gamma$ (black vectors), the flow field (sky-blue vectors) and the surfactant concentration at the interface (red to black corresponding to the variation shown in figure 11, black for 0 wt% corresponding to $\Gamma = 0$). The quadrants show the four different bulk concentrations considered in this paper.

(b) The quantities $\gamma\kappa$ and $100|\nabla_t\gamma|$ along the interface. The abscissa here is the vertical coordinate in (a), such that the left end of this plot corresponds to the pole and the right end to the equator of the drop.

Figure 10: The effect of surfactant concentration on normal and tangential interfacial stress. The plots are for the 0.5 mm diameter drop subjected to a 700 V/mm electric field, at $t = 1$ ms corresponding to the blue vertical line in figure 11. The values of ζ are 0.39, 0.40, 0.44 and 0.59 in order of increasing surfactant concentration.

concentrations Γ_{\min} and Γ_{\max} for each case with surfactant present are plotted in figure 11 as functions of time. For comparison, the maximum possible interfacial concentration given by fitting the Langmuir EoS equation (7) to the experimental data is 1.31×10^{-4} mol/m², and all values are well below this.

In figure 10b we show the two components of the vector $\gamma\kappa\mathbf{n} - 100 \cdot \nabla_t\gamma$ plotted as a function of the vertical coordinate y , covering here one quadrant of the drop. Inspecting the plot, it is seen that the Marangoni forces increase significantly at the lower surfactant concentrations, while the decrease in interfacial tension is significant mainly for the highest surfactant concentration. These plots confirm the hypothesis put forward to explain the influence of surfactants on the damping which is seen in figure 6.

Another interesting phenomenon seen in the numerical results is the effect of

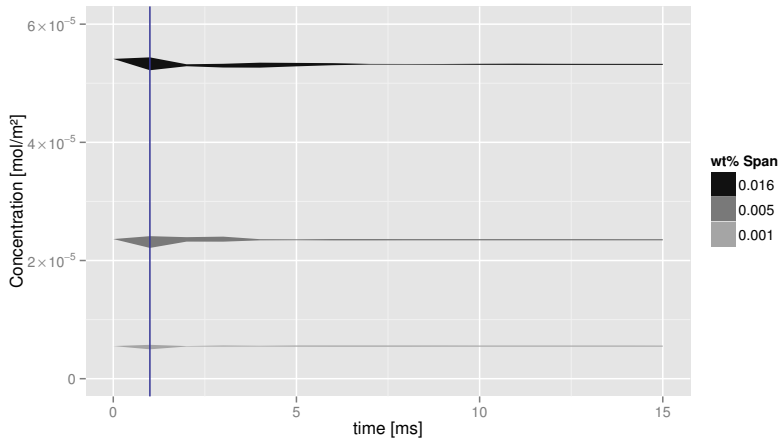


Figure 11: The time evolution of the minimum and maximum interfacial surfactant concentration, shown as the lower and upper edges of shaded bands, for the three cases with surfactants shown in figure 10. The vertical blue line shows the instant at which figure 10 is plotted. Note that all values are well below $\Gamma_\infty = 1.31 \times 10^{-4}$ mol/m², i.e. within the range of validity of the surfactant EoS.

surfactant concentration on the damping of oscillations, cf. figure 6. Naturally, it is interesting to see if the experiments show a similar trend. Since the experimental results do not admit the same direct comparison by holding two parameters identical while varying a third, the electric field was binned into 5 intervals with limits at (200, 400, 500, 600, 700, 800) V/mm. No experiments were done with electric fields below 200 or above 800 V/mm. We then considered all results within such a bin and with a given surfactant concentration and joined these into groups, amounting to averaging over the radius. This gave $5 \times 3 = 15$ groups. We omit deformations where the difference between the maximum and the static deformation was smaller than the optical resolution, i.e. we only consider observably underdamped oscillations.

To create a plot like figure 6, the centre-of-mass of each group was computed, connecting centre-of-mass points that represent groups with the same range of electric fields. This corresponds to averaging over the drop radius. Plotting this together with the simulation results in figure 12, it is seen that a similar trend is found, in particular for the slopes between the 0.001 and 0.005 wt% results. However, the absolute value of the damping is lower

In this comparison, note that the circular points corresponding to zero surfactant can only be shown for the simulation results, since the system is known to be contaminated even when no Span 80 is added. Note also that in the plot of the simulation results, only those drops with $D \geq 600 \mu\text{m}$ are shown in order to reduce clutter.

When it comes to the hysteresis, we have no clear explanation of the observed phenomena. It is evident from the results shown in figure 7 that the simulations

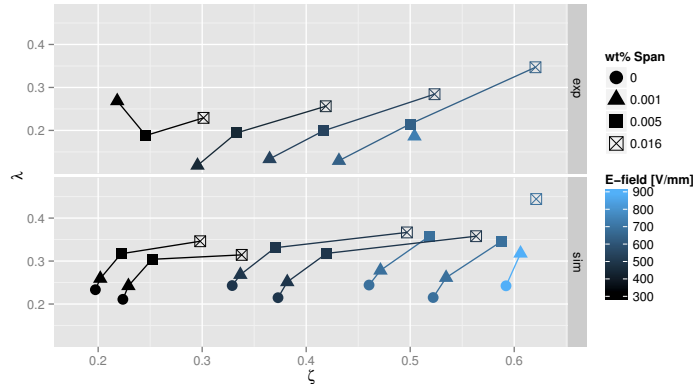


Figure 12: The damping ratio λ versus ζ , for the experimental values (top) and the simulation results shown in figure 6 (bottom). The simulation results are only shown for drops with $D \geq 600\mu\text{m}$ to avoid clutter.

cannot explain the hysteresis, even when taking into account the external flow, the history of previous deformations and the Marangoni effect. There is a possibility that incorporating the elastic effects caused by the surfactant could help explain the hysteresis, but this does not seem to be likely *a priori*, since the forces from the elasticity are expected to decrease the deformation, not increase it. Our results do not appear to support the hypothesis by Peltonen and Yliruusi (2000), where it is proposed that the hysteresis can be explained by the previous deformations causing surfactants to detach into the water phase. If this were the case, we should observe the hysteresis also for falling voltage pulses, and we do not. If one may speculate, it could be that the small deformations caused by the initial part of a rising pulse train can cause a phase transition in the monolayer of surfactants at the interface. Such phenomena have been reported in the literature (Ravera *et al.*, 2005).

5. Concluding remarks

We have performed detailed studies of the effect of surfactants on the electrohydrodynamic stretching of water drops in oil at various drop sizes and electric field strengths, covering the full range of dimensionless electric field ζ from zero to drop breakup. We have compared our results to the classic result by Taylor, which assumes no surfactants present at the drop interface, and predicts the deformation as a function of ζ .

We find that when the equilibrium interfacial tension caused by the surfactant is used in the expression for ζ , the system remains well-described by this dimensionless quantity, as expected from figure 11 which shows that the surfactant maldistribution quickly becomes small. For field strengths below $\zeta \sim 0.4$, i.e. deformations below $a/b \sim 1.12$, we have found only negligible

deviations from the Taylor theory when surfactants are added. For field strengths above this we have reported significant deviations of the observed drop deformations, as well as an ability to go slightly beyond the critical stability limit, $\zeta \sim 0.65$, predicted by the Taylor theory without drops breaking up. The deviations from the Taylor theory are larger for experimental than for the simulation results, which could be explained by the interfacial elasticity caused by the surfactant, an effect which is not taken into account in the simulations.

We have shown both by simulations and experiments that the addition of surfactants damps the oscillations induced by a suddenly applied electric field, an effect which may be attributed to the Marangoni effect that arises in the presence of interfacial-tension gradients. We have studied the effects of the surfactant concentration on the damping of oscillations, and found that low concentrations increase the damping significantly while having little effect on the static deformation. On the other hand, the difference between low and high surfactant concentrations lies mainly in the change of equilibrium surface tension, which affects the static deformation.

Finally we have observed in our experiments a significant hysteresis effect when repeatedly stretching drops at high surfactant concentrations. But these effects are only seen for the case where the applied deformations are first small and then increased, not in the opposite case when the deformations are first large and then decreased. We have investigated whether this effect can be explained just by the hydrodynamics and surfactant transport, and have found this not to be the case. One may speculate that the small initial deformations give the surfactant heads enough room to reorient into an energetically more favorable state, thus making the interface more pliable.

The data produced by the parameter studies in this paper are permanently stored at Figshare, <http://dx.doi.org/10.6084/m9.figshare.1254343>.

Acknowledgments

We would like to thank Dr. Martin Fossen (SINTEF Petroleum Research) for the measurements of interfacial tension as a function of surfactant concentration, Dr. Velaug Myrseth Oltedal (SINTEF Petroleum Research) for the measurements of bulk viscosity, and Dr. Cédric Lesaint (SINTEF Energy Research) for the measurements of density and for enlightening discussions of the interfacial tension measurements. We would also like to thank Dr. Gunnar Berg (SINTEF Energy Research) as well as Professor Jean-Luc Reboud and Dr. Pierre Atten (G2Elab) and Dr. Erik Bjørklund (Sulzer Chemtech) for fruitful discussions on the work presented here.

This work was funded by the project *Fundamental understanding of electrocoalescence in heavy crude oils* coordinated by SINTEF Energy Research. The authors acknowledge the financial support from the Petromaks programme of the Research Council of Norway (206976), Petrobras, Statoil and Sulzer Chemtech.

References

- Adalsteinsson, D., Sethian, J. A., 1999. The fast construction of extension velocities in level set methods. *J. Comput. Phys.* 148 (1), 2 – 22. doi:10.1006/jcph.1998.6090.
- Atten, P., May 1993. Electrocoalescence of water droplets in an insulating liquid. *J. Electrostat.* 30, 259–269. doi:10.1016/0304-3886(93)90080-Q.
- Balay, S., Gropp, W. D., McInnes, L. C., Smith, B. F., 1997. Efficient management of parallelism in object-oriented numerical software libraries. In: Bruaset, A., Arge, E., Langtangen, H. (Eds.), *Modern Software Tools for Scientific Computing*, Springer, pp. 163–202.
- Bjørklund, E., Feb. 2008. The level-set method applied to droplet dynamics in the presence of an electric field. *Comput. Fluids* 28 (2), 358–269. doi:10.1016/j.compfluid.2008.04.008.
- Bond, W. N., Newton, D. A., 1928. LXXXII. Bubbles and drops and Stokes’ law. (Paper 2). *Phil. Mag.* 5 (30), 794–800.
- Brazier-Smith, P. R., 1971. Stability and shape of isolated and pairs of water drops in an electric field. *Phys. Fluids* 14 (1), 1–6. doi:10.1063/1.1693258.
- Chorin, A. J., 1968. Numerical solution of the Navier-Stokes equations. *Math. Comput.* 22 (104), 745–762. doi:10.1090/S0025-5718-1968-0242392-2.
- Clift, R., Grace, J., Weber, M., 1978. *Bubbles, drops and particles*. Academic Press.
- Dukhin, S. S., Kretschmar, G., Miller, R., 1995. *Dynamics of adsorption at liquid interfaces: theory, experiment, application*, vol. 1. Elsevier.
- Eow, J. S., Ghadiri, M., Sharif, A. O., Williams, T. J., 2001. Electrostatic enhancement of coalescence of water droplets in oil: a review of the current understanding. *Chem. Eng. J.* 84 (3), 173–192. doi:10.1016/S1385-8947(01)00250-9.
- Ervik, Å., Hellesø, S. M., Munkejord, S. T., Müller, B., July 2014. Experimental and computational studies of water drops falling through model oil with surfactant and subjected to an electric field. In: *Proceedings of the IEEE 18th International Conference on Dielectric Liquids*. Bled, Slovenia. doi:10.1109/ICDL.2014.6893172.
- Falgout, R., Jones, J., Yang, U., 2006. *The Design and Implementation of hypre, a Library of Parallel High Performance Preconditioners*, Springer-Verlag, pp. 267–294. doi:10.1007/3-540-31619-1_8.
- Fedkiw, R. P., Aslam, T., Merriman, B., Osher, S., Jul. 1999. A non-oscillatory Eulerian approach to interfaces in multimaterial flows (the ghost fluid method). *J. Comput. Phys.* 152 (2), 457–492. doi:10.1006/jcph.1999.6236.

- Gottlieb, S., Ketcheson, D. I., Shu, C.-W., 2009. High order strong stability preserving time discretizations. *J. Sci. Comput.* 38 (3), 251–289. doi:10.1007/s10915-008-9239-z.
- Ha, J.-W., Yang, S.-M., 1998. Effect of nonionic surfactant on the deformation and breakup of a drop in an electric field. *J. Colloid Interf. Sci.* 206 (1), 195 – 204. doi:10.1006/jcis.1998.5676.
- Hadamard, J., 1911. Mouvement permanent lent d’une sphère liquide et visqueuse dans un liquide visqueux. *C. R. Acad. Sci.* 152 (25), 1735–1738.
- Hartmann, D., Meinke, M., Schröder, W., 2010. The constrained reinitialization equation for level set methods. *J. Comput. Phys.* 229 (5), 1514 – 1535. doi:10.1016/j.jcp.2009.10.042.
- Henson, V. E., Yang, U. M., 2000. BoomerAMG: a parallel algebraic multigrid solver and preconditioner. *Appl. Numer. Math.* 41, 155–177. doi:10.1016/S0168-9274(01)00115-5.
- Iwahashi, M., Umehara, A., Wakisaka, K., Kasahara, Y., Minami, H., Matsuzawa, H., Shinzawa, H., Ozaki, Y., Suzuki, M., 2007. Effect of cholesterol and other additives on viscosity, self-diffusion coefficient, and intramolecular movements of oleic acid. *J. Phys. Chem. B* 111 (4), 740–747. doi:10.1021/jp0619538.
- Jiang, G.-S., Peng, D., 2000. Weighted ENO schemes for Hamilton-Jacobi equations. *SIAM J. Sci. Comput.* 21 (6), 2126–2143. doi:10.1137/S106482759732455X.
- Lamb, H., 1932. *Hydrodynamics*. Cambridge University Press, Cambridge, 6th ed.
- Levich, V. G., 1962. *Physicochemical hydrodynamics*. Prentice-Hall, second ed.
- Lin, S.-Y., Lee, Y.-C., Yang, M.-W., Liu, H.-S., 2003. Surface equation of state of nonionic $c_m e_n$ surfactants. *Langmuir* 19 (8), 3164–3171. doi:10.1021/la026574u.
- Lin, S.-Y., McKeigue, K., Maldarelli, C., 1990. Diffusion-controlled surfactant adsorption studied by pendant drop digitization. *AIChE J.* 36 (12), 1785–1795. doi:10.1002/aic.690361202.
- Lucassen-Reynders, E., Cagna, A., Lucassen, J., 2001. Gibbs elasticity, surface dilational modulus and diffusional relaxation in nonionic surfactant monolayers. *Colloids Surf. A* 186 (1–2), 63 – 72. ISSN 0927-7757. doi:S0927-7757(01)00483-6.
- Lundgaard, L. E., Berg, G., Ingebrigtsen, S., Atten, P., 2006. Electrocoalescence for oil-water separation: Fundamental aspects. In: Sjöblom, J. (Ed.), *Emulsions and Emulsion Stability*, Taylor & Francis, vol. 132 of *Surfactant Science Series*, chap. 15, pp. 549–592. Second ed.

- Melcher, J. R., Taylor, G. I., 1969. Electrohydrodynamics: a review of the role of interfacial shear stresses. *Ann. Rev. Fluid Mech.* 1 (1), 111–146. doi:10.1146/annurev.fl.01.010169.000551.
- Moffat, R. J., 1988. Describing the uncertainties in experimental results. *Exp. Therm. Fluid Sci.* 1, 3–17. doi:10.1016/0894-1777(88)90043-X.
- Nganguia, H., Young, Y.-N., Vlahovska, P. M., Bławdziewicz, J., Zhang, J., Lin, H., 2013. Equilibrium electro-deformation of a surfactant-laden viscous drop. *Phys. Fluids* 25 (9), 092106. doi:10.1063/1.4821205.
- Ogata, K., 2009. *Modern Control Engineering*. Prentice Hall, New Jersey, fifth ed.
- Osher, S., Fedkiw, R. P., 2001. Level set methods: An overview and some recent results. *J. Comput. Phys.* 169 (2), 463 – 502. doi:10.1006/jcph.2000.6636.
- Pawar, Y., Stebe, K. J., 1996. Marangoni effects on drop deformation in an extensional flow: The role of surfactant physical chemistry. i. insoluble surfactants. *Phys. Fluids* 8 (7), 1738–1751. doi:10.1063/1.868958.
- Peltonen, L. J., Yliruusi, J., 2000. Surface pressure, hysteresis, interfacial tension, and CMC of four sorbitan monoesters at water–air, water–hexane, and hexane–air interfaces. *J. Colloid Interf. Sci.* 227 (1), 1 – 6. ISSN 0021-9797. doi:10.1006/jcis.2000.6810.
- Prosperetti, A., 1980. Free oscillations of drops and bubbles: the initial-value problem. *J. Fluid Mech.* 100 (02), 333–347. doi:10.1017/S0022112080001188.
- Ravera, F., Ferrari, M., Santini, E., Liggieri, L., 2005. Influence of surface processes on the dilational visco-elasticity of surfactant solutions. *Adv. Colloid Interf. Sci.* 117 (1–3), 75 – 100. doi:10.1016/j.cis.2005.06.002.
- Rybzynski, W., 1911. Über die fortschreitende Bewegung einer flüssigen Kugel in einem zähen Medium. *Bull. Acad. Sci. Cracovie* .
- Sakata, E., Berg, J., 1969. Surface diffusion in monolayers. *Ind. & Eng. Chem. Fundam.* 8 (3), 570–575. doi:10.1021/i160031a033.
- Saville, D. A., 1997. Electrohydrodynamics: The Taylor-Melcher leaky dielectric model. *Ann. Rev. Fluid Mech.* 29 (1), 27–64. doi:10.1146/annurev.fluid.29.1.27.
- Sherwood, J. D., 1988. Breakup of fluid droplets in electric and magnetic fields. *J. Fluid Mech.* 188, 133–146. doi:10.1017/S0022112088000667.
- Stokes, G. G., 1851. On the effect of the internal friction of fluids on the motion of pendulums. *Trans. Camb. Phil. Soc.* 9, 8.

- Sunder, S., Tomar, G., 2016. Numerical simulations of bubble formation from a submerged orifice and a needle: The effects of an alternating electric field. *Eur. J. Mech. B/Fluids* 56, 97–109. doi:10.1016/j.euromechflu.2015.11.014.
- Szyszkowski, B., 1908. Experimentelle Studien über kapillare Eigenschaften der wässerigen Lösungen von Fettsäuren. *Z. Phys. Chem.* 64, 385–414.
- Taylor, G., 1964. Disintegration of water drops in an electric field. *Proc. R. Soc. A* 280 (1382), 383–397. doi:10.1098/rspa.1964.0151.
- Teigen, K. E., Lervåg, K. Y., Munkejord, S. T., 2010. Sharp interface simulations of surfactant-covered drops in electric fields. In: *Fifth European Conference on Computational Fluid Dynamics, ECCOMAS CFD 2010*. ISBN 978-989-96778-1-4.
- Teigen, K. E., Munkejord, S. T., Apr. 2009. Sharp-interface simulations of drop deformation in electric fields. *IEEE T. Dielect. El. In.* 16 (2), 475–482. doi:10.1109/TDEI.2009.4815181.
- Teigen, K. E., Munkejord, S. T., Nov. 2010. Influence of surfactant on drop deformation in an electric field. *Phys. Fluids* 22 (11). doi:10.1063/1.3504271. Article 112104.
- Tsujii, K., 1998. *Surface Activity: Principles, Phenomena, and Applications*. Academic Press.
- van der Vorst, H., 1992. Bi-CGSTAB: A fast and smoothly converging variant of Bi-CG for the solution of nonsymmetric linear systems. *SIAM J. Sci. Comput.* 13 (2), 631–644. doi:10.1137/0913035.
- White, F. M., 2009. *Fluid Mechanics*. McGraw-Hill, 6th ed.
- Xu, J.-J., Li, Z., Lowengrub, J., Zhao, H., 2006. A level-set method for interfacial flows with surfactant. *J. Comput. Phys.* 212 (2), 590–616. doi:10.1016/j.jcp.2005.07.016.
- Zhang, L., He, L., Ghadiri, M., Hassanpour, A., 2015. Effect of surfactants on the deformation and break-up of an aqueous drop in oils under high electric field strengths. *J. Petrol. Sci. Eng.* 125, 38 – 47. doi:10.1016/j.petrol.2014.11.014.
- Zhao, H., 2009. *An Experimental Investigation of Liquid Droplets Impinging Vertically on a Deep Liquid Pool*. Ph.D. thesis, NTNU.